Am J Physiol Renal Physiol 306: F309–F320, 2014.
First published December 11, 2013; doi:10.1152/ajprenal.00519.2013.

ENaC activity is increased in isolated, split-open cortical collecting ducts from protein kinase Cα knockout mice

Hui-Fang Bao,[1,2] Tiffany L. Thai,[1,2] Qiang Yue,[1,2] He-Ping Ma,[1,2] Amity F. Eaton,[1,2] Hui Cai,[1,2,3] Janet D. Klein,[1,2,3] Jeff M. Sands,[1,2,3] and Douglas C. Eaton[1,2]

[1]*Department of Physiology, Emory University School of Medicine, Atlanta, Georgia;* [2]*The Center for Cell and Molecular Signaling, Emory University School of Medicine, Atlanta, Georgia; and* [3]*Department of Medicine, Renal Division, Emory University School of Medicine, Atlanta, Georgia*

Submitted 23 September 2013; accepted in final form 4 December 2013

Bao HF, Thai TL, Yue Q, Ma HP, Eaton AF, Cai H, Klein JD, Sands JM, Eaton DC. ENaC activity is increased in isolated, split-open cortical collecting ducts from protein kinase Cα knockout mice. *Am J Physiol Renal Physiol* 306: F309–F320, 2014. First published December 11, 2013; doi:10.1152/ajprenal.00519.2013.—The epithelial Na channel (ENaC) is negatively regulated by protein kinase C (PKC) as shown using PKC activators in a cell culture model. To determine whether PKCα influences ENaC activity in vivo, we examined the regulation of ENaC in renal tubules from PKCα$^{-/-}$ mice. Cortical collecting ducts were dissected and split open, and the exposed principal cells were subjected to cell-attached patch clamp. In the absence of PKCα, the open probability (P_o) of ENaC was increased three-fold vs. wild-type SV129 mice (0.52 ± 0.04 vs. 0.17 ± 0.02). The number of channels per patch was also increased. Using confocal microscopy, we observed an increase in membrane localization of α-, β-, and γ-subunits of ENaC in principal cells in the cortical collecting ducts of PKCα$^{-/-}$ mice compared with wild-type mice. To confirm this increase, one kidney from each animal was perfused with biotin, and membrane protein was pulled down with streptavidin. The nonbiotinylated kidney was used to assess total protein. While total ENaC protein did not change in PKCα$^{-/-}$ mice, membrane localization of all the ENaC subunits was increased. The increase in membrane ENaC could be explained by the observation that ERK1/2 phosphorylation was decreased in the knockout mice. These results imply a reduction in ENaC membrane accumulation and P_o by PKCα in vivo. The PKC-mediated increase in ENaC activity was associated with an increase in blood pressure in knockout mice fed a high-salt diet.

protein kinase Cα; ENaC; renal tubules; single channels; knockout mice; hypertension

EPITHELIAL NA CHANNELS (ENaC) are sodium-permeable ion channels located in the apical membrane of polarized epithelial cells primarily in the distal nephron, lung, and distal colon. In the distal nephron, ENaC activity is the rate-limiting step for Na^+ reabsorption (16, 34); therefore, ENaC activity is critical for the physiological maintenance of systemic Na^+ homeostasis and long-term control of blood pressure. Because of its central role in responding to changes in Na^+ uptake, ENaC activity is tightly regulated; dysregulation of this channel has been linked to abnormal blood pressure in several genetic disorders including Liddle's syndrome (18, 37) and pseudohypoaldosteronism type 1 (9, 33, 41).

Address for reprint requests and other correspondence: D. C. Eaton, Emory Univ. School of Medicine, Dept. of Physiology, Whitehead Biomedical Research Bldg., 615 Michael St., Atlanta, GA 30322 (e-mail: deaton@emory.edu).

ENaC can be regulated either by altering the amount of time the channel spends open (open probability or P_o) or by altering the density of functional channels (N) in the apical membrane of distal nephron epithelial cells. One signaling molecule that appears to alter ENaC activity is protein kinase C (PKC). Activation of PKC with phorbol esters reduces ENaC activity in the apical membrane of A6 cells, an amphibian renal cell line, and in rat principal cells (15). In contrast to the inhibitory effect on ENaC due to activating PKC, pharmacologically inhibiting PKC increases ENaC P_o (23, 49). A6 cells, on which many of the experiments described above were performed, contain several different PKC isoforms; so that it is difficult to determine which isoform is responsible for the changes in ENaC activity after stimulation or inhibition of all the PKC isoforms. There are conflicting reports in the literature about which isoforms of PKC are present in principal cells of the mouse cortical collecting duct. One report suggested that, in mice, there was no PKC present in principal cells (29); subsequent work suggested that PKCα was present, but no other typical or novel isoforms (22). Therefore, we made use of PKCα knockout mice to examine PKC regulation of ENaC in isolated split-open collecting duct principal cells.

METHODS

Animals. PKCα$^{-/-}$ mice were initially graciously obtained from the laboratory of Jeffery Molkentin at the University of Cincinnati (17) and maintained in house. Control mice were developed from backcrossing PKCα$^{-/-}$ mice to SV129 controls 10 times to obtain littermate wild-type animals. Once established, the wild-type control line was maintained and used as controls for the PKCα knockouts. Mice were kept on a 12:12-h light-dark cycle and fed standard laboratory chow and tap water ad libitum. Mice fed a high-salt diet were fed standard laboratory chow containing 8% NaCl in place of standard chow ad libitum for 14–21 days before euthanasia. All of our animal protocols and procedures in this paper were approved by the Emory Institutional Animal Care and Use Committee.

Blood pressure measurements. Systolic blood pressure and heart rate were measured by tail cuff as previously described (43). Blood pressures were measured for 5 consecutive days before and during *weeks 1* and *2* of a high-salt diet. Data from the first 2 days of each cycle were discarded as this was considered a transition period in which the mice become accustomed to the procedure. Between measurement times, mice were allowed to rest for 2 days to avoid extraordinarily high stress levels. Blood pressures were measured on a warmed platform (BP-2000, Visitech Systems), and mice were allowed to rest on the platform for 15 min before measurement. Five preliminary measurements were made and discarded to accustom mice to the procedure. Blood pressures and heart rates are an average of 10 measurements each day.

SDS-PAGE and immunoblotting. Freshly isolated kidneys were minced and washed once with PBS and then homogenized using an Omni TH homogenizer (Warrenton, VA) in tissue protein extraction reagent (TPER; Thermo Scientific), both solutions containing protease and phosphatase inhibitors (Thermo Scientific). Tissue lysates were centrifuged at 1,000 rpm at 4°C for 10 min to remove debris. The supernatant was then centrifuged at 18,000 *g* for 6 h to sediment a total membrane fraction; this pellet was suspended in a 150-μl lysis buffer. Protein concentration was calculated for cell and tissue lysates using the BCA protein assay (Thermo Scientific). Forty micrograms of total protein prepared in Laemmli sample buffer (Bio-Rad, Hercules, CA) was loaded and resolved on Bio-Rad Any KD gradient gels using the Criterion or Protean electrophoresis systems (Bio-Rad). The separated proteins were electrically transferred onto Immobilon-P transfer membranes (Millipore, Billerica, MA). The membranes were blocked in 5% wt/vol milk in TBST (Bio-Rad) at room temperature for 1 h. The membranes were washed once with TBST and then incubated with primary antibodies at a dilution of 1:1,000 in 5% wt/vol milk in TBST at 4°C for 8 h. The membranes were washed three times with TBST for 5-min intervals before being incubated with horseradish peroxidase-conjugated goat anti-rabbit secondary antibody at a dilution of 1:5,000 in blocking solution. The membranes were incubated with SuperSignal Dura Chemiluminescent Substrate for 5 min before being developed using a Kodak Gel Logic 2200 Imager and Molecular Imaging software (Carestream Health, Rochester, NY). This method was used to detect ENaC subunits (with in-house antibodies) (1, 4, 8, 40, 46), ERK1/2 (9102, Cell Signaling) and phosphoERK1/2 (9101a, Cell Signaling). PKC isoforms were detected with antibodies obtained from Cell Signaling, (In particular, PKCα was detected with Cell Signaling no. 9375.)

Antibody production. Restricted segments of the α (H554-N643)- and β-C terminus (D566-N647) were subcloned into the pGEX expression vector. A segment of the α-extracellular domain ^{250}KIGFQ. . . . SNLWMS^{347} from a rat was subcloned into a maltose-binding-protein vector. The constructs were transformed into competent bacterial cells, induced with IPTG for expression, and batch purified from inclusion bodies using glutathione Sepharose 4B (2, 3) or an amylose column. A peptide corresponding to ^{599}CVDNPI . . . RIQSAF^{647} from the *Xenopus* γ-subunit was synthesized. The subunit-specific antibodies were raised in rabbits against a synthetic peptide sequence or fusion proteins described above. Polyclonal antibodies against the carboxy terminal domain of α-ENaC (ENaC 59) and β-ENaC (ENaC 60) and the extracellular domain of α (890)- and the C-terminal domain of γ (2102) were generated in White New Zealand rabbits by Bio-Synthesis (Lewisville, TX). Each batch of serum was supplemented with sodium azide and evaluated for specificity and cross-reactivity using protein from the wheat germ in vitro translation system (Promega) and mouse renal tissue lysates.

Single-channel patch clamp. Renal tubules were manually dissected, and the cortical collecting duct was identified by morphology. Tubules were placed in physiological saline [(in mM) 140 NaCl, 5 KCl, 1 $CaCl_2$, and 10 HEPES adjusted to pH 7.4 with NaOH] in a plastic dish before being split open to reveal the apical surface of the cells before single-channel patch clamp as previously described for patch clamp of cells in culture (6, 40, 45, 46, 49). Briefly, a microelectrode was filled with physiological buffer solution in which lithium was substituted for sodium (in mM: 140 LiCl, 5 KCl, 1 $CaCl_2$, and 10 HEPES adjusted to pH 7.4 with NaOH) and lowered to a single cell before application of a small amount of suction to achieve a >1 GΩ seal. ENaC were identified by characteristic channel kinetics (long mean open and closed times >0.5 s) and the current-voltage relationship of the channel (unit conductance close to 6 pS and a very positive, >40 mv, reversal potential).

Measurement of plasma aldosterone. Blood samples were taken from anesthetized mice. Blood samples were extracted with 4× volume of methylene chloride three times before evaporating the solvent under dry nitrogen. The extracted samples were then prepared for ELISA according to the manufacturer's instructions (aldosterone EIA kit- monoclonal, Cayman Biologicals). Plasma aldosterone was calculated by comparison with a standard curve prepared from known concentrations of aldosterone.

In situ biotinylation. For in situ biotinylation, a protocol established by Frindt and Palmer (12, 14) for biotinylation in rats was modified for use in mice. Mice were anesthetized by injection of 40–50 mg/kg pentobarbital sodium (ip). The abdominal cavity was opened to the diaphragm, and a butterfly needle was inserted into the abdominal aorta at the bifurcation of the iliac arteries. The aorta was tied above the level of the renal arteries, and the left renal vein was cut to allow exit of perfusate. The mouse was then moved to an ice bath for cold perfusion. Both kidneys were perfused with PBS for 10 min, after which the left renal artery and vein were tied and the left kidney was removed to serve as a nonbiotinylated control. The right renal vein was then cut, and the right kidney was perfused with PBS containing 0.5 mg/ml sulfosuccinimidyl-2-[biotinamido]ethyl-1,3-dithiopropionate (Pierce) for 15 min, after which a biotin-quenching solution (PBS in which 25 mM Tris·HCl replaced 25 mM NaCl) was perfused for 25 min to remove excess biotin. Whole kidneys were homogenized, and protein was extracted in buffer containing 250 mM sucrose and 10 mM triethanolamine (pH 7.4). The supernatant was then centrifuged at 18,000 *g* for 6 h at 4°C to sediment a total membrane fraction; this pellet was suspended in a 150-μl lysis buffer. The membrane fraction was equally loaded on streptavidin beads (high-capacity neutravadin-agarose resin, Thermo Scientific) and incubated overnight. Beads were washed with a solution of 150 mM NaCl, 5 mM EDTA, 50 mM Tris, and 1% Triton X-100 (pH 7.4) three times followed by a high-salt wash (wash buffer with 500 mM NaCl) and two no-salt washes (10 mM Tris, pH 7.4) to remove unbound protein. Bound protein was eluted in sample buffer containing 0.5 M DTT. Biotinylated and unbiotinylated membrane fractions were run on Bio-Rad Any KD gradient gels and probed with in-house antibodies to α-, β-, or γ-ENaC.

Fluorescent immunohistochemistry. Fluorescent immunohistochemistry was performed as previously described (43, 45). Briefly, kidneys were perfused in situ with PBS followed by 2% paraformaldehyde. Kidneys were removed, put in 20% sucrose solution at 4°C overnight, dehydrated, and embedded in paraffin wax. Four-micrometer sections were made, and slices were rehydrated before addition of in-house ENaC or aquaporin-2 (AQP2) antibodies or commercially available antibodies against PKCα (SC-8393, Santa Cruz Biotechnology). Antibodies were detected using an appropriate fluorescently conjugated secondary antibody (Molecular Probes).

Colocalization analysis. To determine whether ENaC subunits colocalize more strongly with AQP2 in knockout mice compared with wild-type, kidney slices from wild-type and knockout mice were stained with rabbit primary antibodies to α-, β-, or γ-ENaC and goat anti-AQP2. Following treatment with fluorescent secondary antibodies, ENaC (green) and AQP2 (red) were examined using confocal microscopy on an Olympus Fluoview 1000 confocal microscope. To determine colocalization, we first determined that there was no fluorescence bleed through from the green channel to the red channel or vice versa. Then we merged images from the green channel and the red channel; yellow in the merged image was an indication of colocalization. To produce a more quantitative measure of the colocalization, we used the colocalization algorithms in the image analysis program ImageJ (11, 28, 35). These algorithms examine the merged images pixel by pixel for red and green intensities and establish thresholds for intensity below which there is no significant correlation of red and green. This represents an unbiased method for determining thresholds. Pixels that have both red and green intensities above the thresholds are analyzed and recolored white. In addition, the number and fraction of pixels with red-green colocalization were calculated and red-green and green-red correlation coefficients were calculated (Manders coefficients, m_1 and m_2) according to *Eq. 1*

$$m_1 = \frac{\sum_i s1_i \cdot s2_i}{\sum_i (s1_i)^2} \quad m_2 = \frac{\sum_i s1_i \cdot s2_i}{\sum_i (s2_i)^2} \qquad (1)$$

where $s1_i$ and $s2_i$ are the red and green intensities of the ith pixel in the image. Only pixels with significant intensities in both channels will contribute to the coefficient.

Data analysis and statistics. All data acquisition and analysis were performed as described previously (45, 47). Data are reported as means ± SE. Statistical analysis was performed with SigmaPlot and SigmaStat software (Jandel Scientific). Differences between groups were evaluated with one-way ANOVA or for blood pressure with two-way ANOVA, and results were considered significant if $P < 0.05$.

We used the FIJI variant of the image-analysis program ImageJ to analyze changes in Western blots. ImageJ calculates the cumulative sum of pixel values above baseline for specific bands in a blot. We averaged these cumulative pixel values for at least three experiments to determine whether there was a significant difference in band densities.

RESULTS

Channels in isolated, split-open tubules. Figure 1*A* shows an isolated tubule before (*top*) and after one end of the tubule from a wild-type SV-129 mouse kidney was split open. A patch electrode on a principal cell is visible in the *bottom left* of the image. Principal cells were identified by their characteristic morphology in the split-open tubule. Specifically, in Fig. 1*A*, principal cells appear in the Hoffman modulation image to be large, polygonal, or round cells with concave surfaces; intercalated cells have asymmetric shapes with convex, but convoluted surfaces. Figure 1*B* shows single-channel records from the patch electrode on the cell in Fig. 1*A*. The currents are inward with long mean open and mean closed times characteristic of ENaC. Figure 1*C* shows the current-voltage relationship for the channel in Fig. 1*B*. The inward rectification and the highly positive reversal potential are also characteristic of ENaC. The conductance of the channel between −100 and 0 mV was 13.1 ± 1.43 pS, similar to that reported in rat connecting tubules by Frindt and Palmer (13).

PKCα knockout mice. We used mice in which PKCα is globally knocked out to study the effect of PKCα on ENaC activity in renal principal cells. Western blotting could not detect PKCα in kidney lysates from knockout mice (Fig. 2, *left*). Immunohistochemistry showed that SV-129 wild-type mice ubiquitously express PKCα in the kidney including in AQP2 (a marker for cortical collecting duct principal cells)-positive cells (Fig. 2, *top right*). As expected, the knockout mice have no detectable PKCα, and, in particular, have none in AQP2-positive principal cells (Fig. 2, *bottom right*). In data not shown, we blotted renal cortical lysates for at least one isoform from each of the major PKC types: typical, novel, and atypical. As expected, we detected low levels of some other PKC isoforms; but, except for PKCα, there was no difference in the isoforms between wild-type and knockout kidneys, implying that there was no compensation of other PKC isoforms for the loss of PKCα.

ENaC activity in PKCα knockout mice on a normal-salt diet. ENaC activity was recorded from cell-attached patches on principal cells (as in Fig. 1) from wild-type mice or from PKCα knockout mice fed a normal mouse diet (Fig. 3*A*). The *top* two traces are long representative records from tubular cells from wild-type or knockout tubules. ENaC activity in the knockout cells is substantially increased above that in the wild-type. The regions marked 1 and 2 in the *top* records are expanded in the two *bottom* traces, which also show that the activity of ENaC in knockout mice is substantially higher than in wild-type mice. Figure 3, *B–D*, summarizes the results from patches on a large number of tubules from both wild-type and knockout mice. Wild-type data are from 31 individual patches; knockout data are from 21 individual patches. The patches were from 21 cortical collecting ducts isolated from wild-type

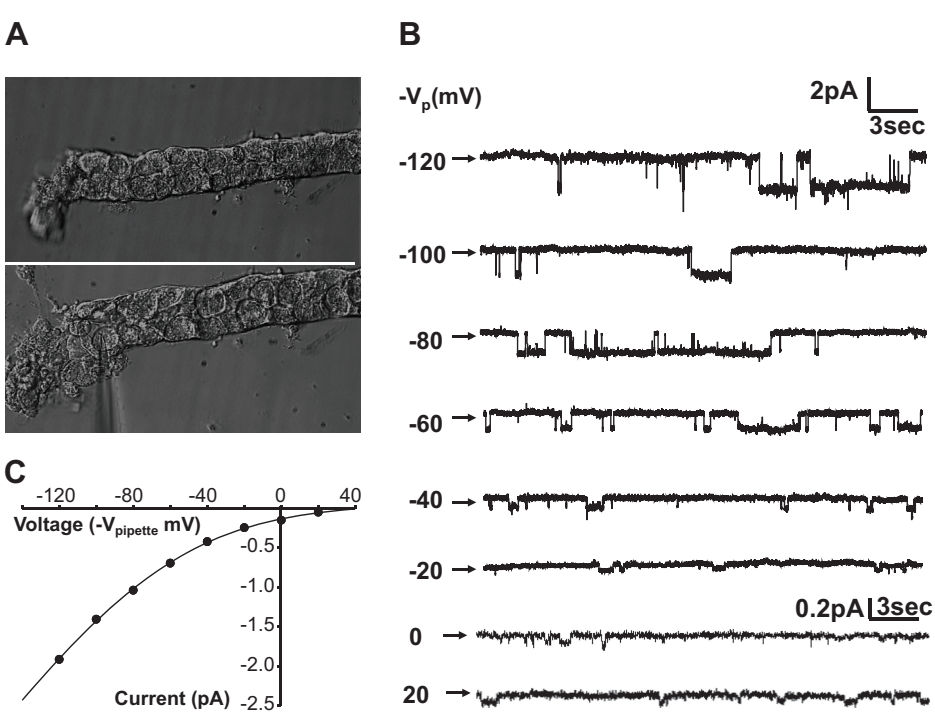

Fig. 1. Channels in isolated, split-open tubules. *A*: an isolated tubule before (*top*) and after splitting open of one end of a tubule from a wild-type SV-129 mouse kidney. A patch electrode on a principal cell is visible in the *bottom left* of the image. Principal cells were identified by their characteristic morphology. *B*: single-channel records from the patch electrode on the cell in *A*. The currents are inward with long mean open and mean closed times characteristic of epithelial sodium channels (ENaC). Note that the vertical scale has been expanded 10-fold for the *bottom* 2 traces to more easily show the small unitary currents at these potentials. *C*: current-voltage relationship for the channel in *B*. The inward rectification and the very positive reversal potential are also characteristic of ENaC. The line through the data is the best nonlinear least-squares fit to the Goldman-Hodgkin-Katz equation and predicts that intracellular sodium is 12 ± 6.6 mM and principal cell sodium permeability is (6.4 ± 3.38) × 10^{-7}cm/s. The conductance of the channel between −100 and 0 mV was 13.1 ± 1.43 pS, similar to that reported in rat connecting tubule by Frindt and Palmer (13).

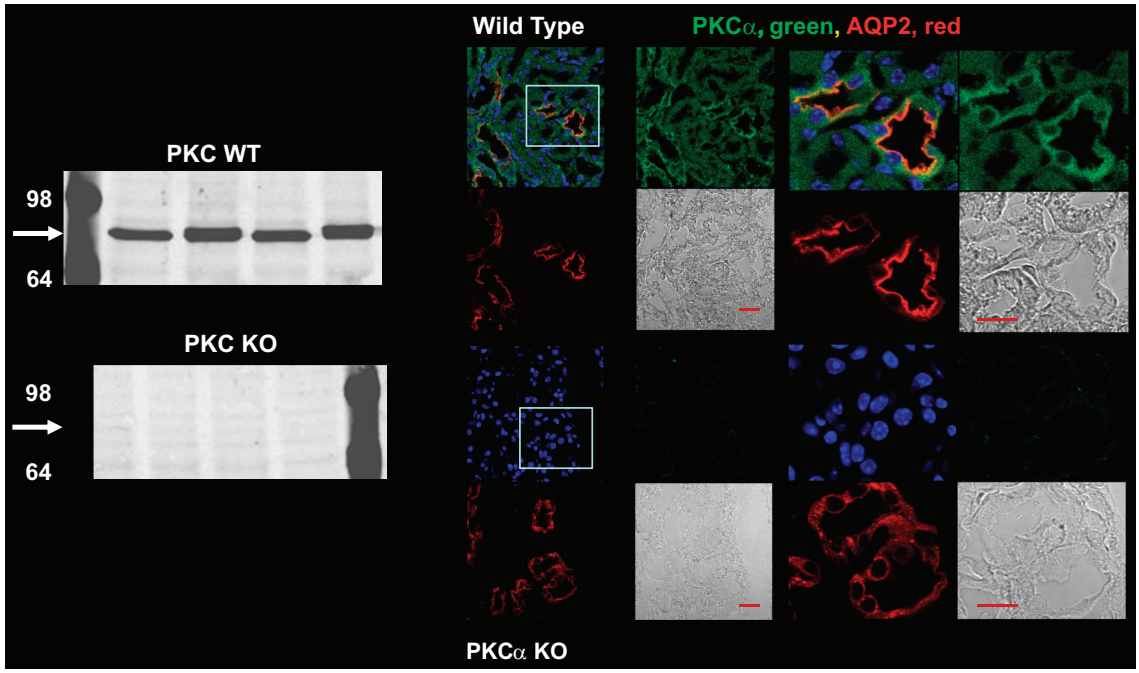

Fig. 2. PKCα knockout mice. *Left*: Western blots of renal cortical lysates from wild-type (WT) and PKCα knockout (KO) mice showing that the knockout mice have no PKCα. The expected molecular weight is 80–82 KDa. Twenty-five micrograms of lysate were loaded per well. *Right*: immunohistochemistry shows that SV-129 WT mice ubiquitously express PKCα in the kidney including in aquaporin-2 (AQP2; a marker for cortical collecting duct principal cells)-positive cells (*top*). The *bottom* panels show mice in which PKCα is globally knocked out. As expected, the KO mice have no detectable PKCα, and, in particular, have none in AQP2-positive principal cells. Scale bars (red lines) = 5 μm in all panels.

and 18 cortical collecting ducts from PKCα knockout mice. The cortical collecting ducts were obtained from 14 wild-type mice and 10 PKCα knockout mice. ENaC activity, measured as NP_o, the product of the number of channels (N) times P_o, is increased more than threefold in knockout tubules compared with wild-type (Fig. 3*B*). When we examined the individual components of activity, we found that P_o more than doubled (Fig. 3*C*). Given prior reports describing the effects of PKC inhibitors, this increase in P_o was not too surprising. What was somewhat surprising to us was that the number of channels per

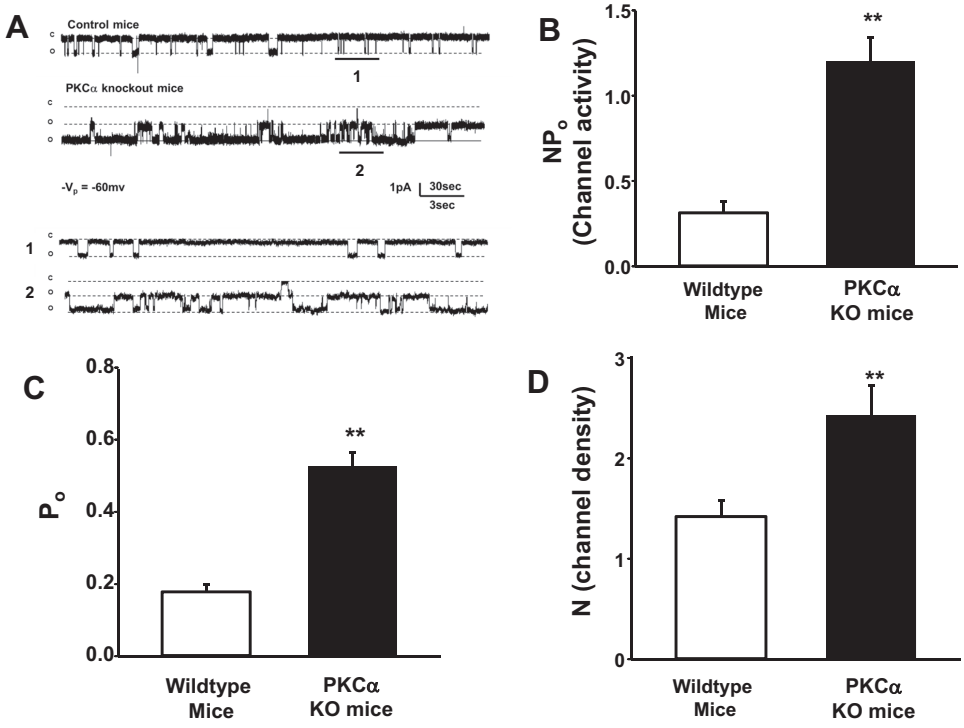

Fig. 3. ENaC activity in PKCα KO mice. ENaC activity was recorded from cell-attached patches on principal cells (as in Fig. 1) from WT mice or PKCα KO mice. *A*: *top* 2 traces are long representative records from WT or KO cells (pipette potential is +60 mv). The activity of the KO cell is substantially increased above that of WT. The regions marked 1 and 2 in the *top* traces are expanded 10-fold in the *bottom* traces to emphasize the difference in the activity of WT and KO cells. All recordings were made at −60 mV (difference in potential between the inside of the cell and the patch pipette. If there is a significant basal membrane potential, it will add to the pipette potential). *B–D*: summary of all single-channel data. The graph in *B* shows that ENaC activity [NP_o; measured as the number of channels (N) times the open probability (P_o)] increases over 3-fold in the PKCα KO mice compared with WT ($P < 0.001$). When the components of activity are examined individually, both P_o (*C*) and N (*D*) increase significantly ($P < 0.01$). WT data are from 31 individual patches; KO data are from 21 individual patches. The patches were from 21 cortical collecting ducts isolated from WT and 18 cortical collecting ducts from PKCα KO. The cortical collecting ducts were obtained from 14 WT mice and 10 PKCα KO mice.

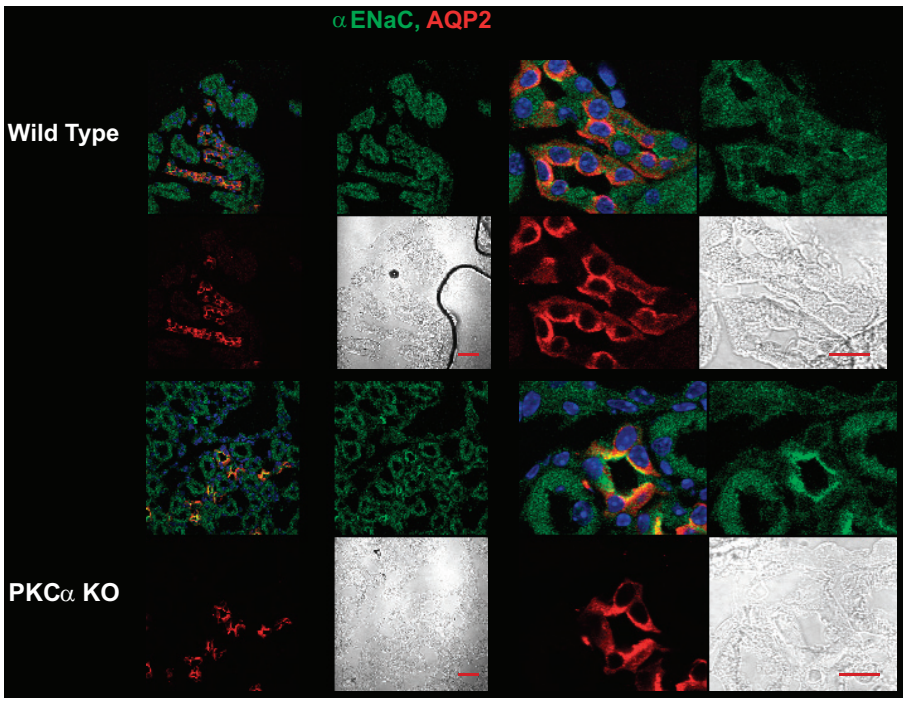

Fig. 4. Membrane α-ENaC is increased in the principal cells of PKCα knockout mice. We prepared kidney slices from WT and KO before fixing and treating with AQP2 and α-ENaC antibodies. Subsequently, we used secondary antibodies that labeled AQP2 with a ds-Red monomer and α-ENaC with enhanced green fluorescent protein. *Left*: 4 panels are, from *bottom right*, differential interference contrast images, AQP2 in red, merged image, and α-ENaC in green. *Right*: expanded images from the areas outlined in white in the merged images on the *left*. α-ENaC appears to more strongly colocalize (yellow) with AQP2 in the principal cells from PKCα KO mice than in WT mice. Scale bars (red lines) = 5 μm in all panels.

patch also increased substantially (Fig. 3*D*). Therefore, we decided to more carefully examine this increase in *N*.

Knocking out PKCα increases the density of ENaC in or near the apical membrane of principal cells. An increase in the number of active channels in the apical membrane could be due to recruitment of new channels to the apical membrane or the conversion of otherwise silent channels to active channels. In the latter case, the number of channels in or near the apical membrane would not change; in the former case, there should be more ENaC near the apical membrane of principal cells. To examine which possibility seemed more likely, we used immunohistochemistry and confocal microscopy of kidney slices to examine the number and localization of ENaC subunits in the apical membranes of AQP2-positive cells. Figure 4 shows that, in knockout compared with wild-type animals, α-ENaC is more strongly colocalized with AQP2 (indicated in yellow) in, or very near, the apical membranes of cells that we presume are principal cells because of the AQP2 staining. Figures 5 and 6

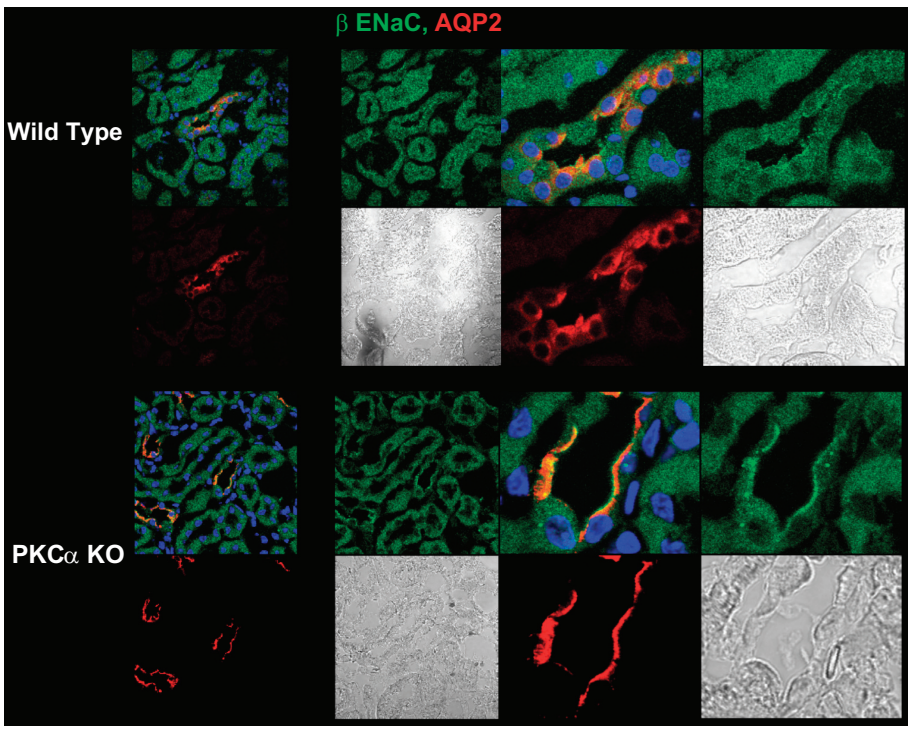

Fig. 5. Membrane β-ENaC is increased in the principal cells of PKCα KO mice. We prepared kidney slices from WT and KO before fixing and treating with AQP2 and β-ENaC antibodies. Subsequently, we used secondary antibodies that labeled AQP2 with a ds-Red monomer and β-ENaC with enhanced green fluorescent protein. *Left*: 4 panels are, from *bottom right*, differential interference contrast images, AQP2 in red, merged image, and β-ENaC in green. *Right*: expanded images from the areas outlined in white in the merged images on the *left*. β-ENaC appears to more strongly colocalize (yellow) with AQP2 in the principal cells from PKCα KO mice than in WT mice. Scale bars (red lines) = 5 μm in all panels.

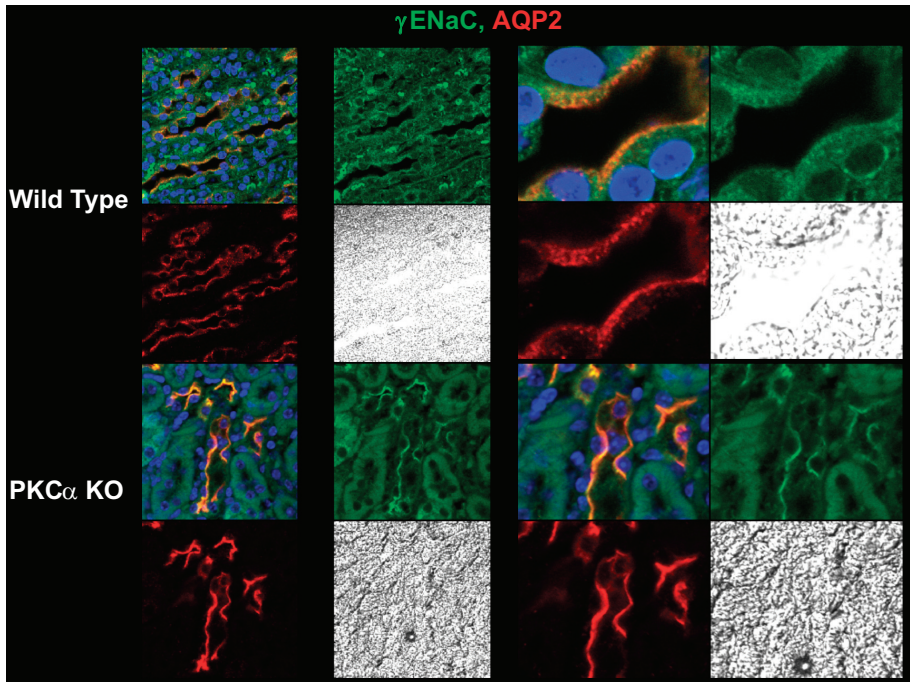

Fig. 6. Membrane γ-ENaC is increased in the principal cells of PKCα knockout mice. We prepared kidney slices from WT and KO before fixing and treating with AQP2 and γ-ENaC antibodies. Subsequently, we used secondary antibodies that labeled AQP2 with a ds-Red monomer and γ -ENaC with enhanced green fluorescent protein. *Left*: 4 panels are, from *bottom right*, differential interference contrast images, AQP2 in red, merged image, and γ-ENaC in green. *Right*: expanded images from the areas outlined in white in the merged images on the *left*. γ-ENaC appears to more strongly colocalize (yellow) with AQP2 in the principal cells from PKCα KO mice than in WT mice. Scale bars (red lines) = 5 μm in all panels.

show that β- and γ-ENaC are also more strongly associated with the apical membrane and AQP2 in principal cells from knockout animals.

Although the yellow color of the merged images in Figs. 4–6 suggests that there is more colocalization of ENaC and AQP2 in the knockout mice, we wanted a more quantifiable measure of colocalization. Therefore, we used the image-analysis program ImageJ to quantify colocalization (as described in METHODS). Figure 7 shows, for slices from wild-type and knockout mice, the merged images for AQP2 and each ENaC subunit; to the *right* of the merged images are merged images in which pixels that have significant red and green intensities have been recolored white. There is more colocalization in the knockout mice than in wild-type. Table 1 gives actual values for the red-green and green-red overlap and the number and percentage of pixels with significant overlap. Association of the red channel (AQP2) with the green channel (ENaC subunits) was calculated using the colocalization plugin of ImageJ. The last two columns show that ENaC is significantly more likely to be associated with ENaC in the knockout mice compared with wild-type ($P < 0.001$ for all subunits). Examination of the red-green and green-red localization shows that AQP2 is almost always associated with an ENaC subunit, but that ENaC subunits (particularly in wild-type mice) are less likely to be associated with AQP2. We interpret these results to imply that ENaC moves in knockout mice to regions of the cell near AQP2, i.e., near the apical membrane. The percent values for knockout vs. wild-type are significantly different ($P < 0.001$ for each subunit by z-test).

Although confocal microscopy makes it appear possible that ENaC is concentrated in the apical membranes of principal cells in knockout animals, we could not rule out the possibility that ENaC subunits were very close to the inner surface of the apical membranes, but not actually in the membrane as parts of active channels. Therefore, we adapted an approach previously used in rats (12, 14) to mice in which we perfused one kidney with biotin to label proteins on the luminal surface of the tubules and confirm that ENaC is actually in the apical membrane (Fig. 8*A*). After precipitating biotin-labeled proteins from kidney lysates, we resolved the avidin precipitates and blotted for the three ENaC subunits (Fig. 8*B*). The quantity of each of the subunits was increased in the PKCα knockout mice, confirming that indeed ENaC was increased in the apical membranes of principal cells as we had shown in the confocal images (Fig. 8*C*).

Plasma aldosterone in PKCα knockout mice is not significantly different from wild-type mice. The increase in P_o and channel density could be explained if plasma aldosterone levels were substantially elevated in PKCα knockout mice. Therefore, we took blood samples from 24 mice (10 wild-type and 7 knockout animals on a normal diet; 3 wild-type and 4 knockout on a high-salt diet). After sample preparation, plasma aldosterone was determined using a commercially available enzyme-linked immunoassay kit. As we anticipated, because a normal mouse diet contains moderate amounts of salt and a high-salt diet even more, aldosterone levels were low but not significantly different in wild-type or knockout mice [normal diet wild-type = 0.57 ± 0.14 nM (n = 10) vs. knockout = 0.76 ± 0.20 nM (n = 7); high-salt diet wild-type = 0.54 ± 0.24 nM (n = 3) vs. knockout = 0.33 ± 0.21 nM (n = 4; means ± SE)]. Therefore, differences in aldosterone concentration cannot explain the increase in ENaC activity in PKCa knockout mice.

ERK1/2 activity is reduced in PKCα knockout mice. ENaC density in the apical membrane is controlled by the activity of the ubiquitin ligase Nedd4-2 (39, 53). The ability of Nedd4-2 to ubiquitinate ENaC and promote internalization is augmented by PKC-mediated ERK1/2 phosphorylation of ENaC (7). Therefore, we examined ERK1/2 phosphorylation as a measure of ERK1/2 activity in wild-type and PKCα knockout mice. We found that the ERK1/2 amount was unchanged, but phosphorylation was significantly reduced in knockout mice (Fig. 9).

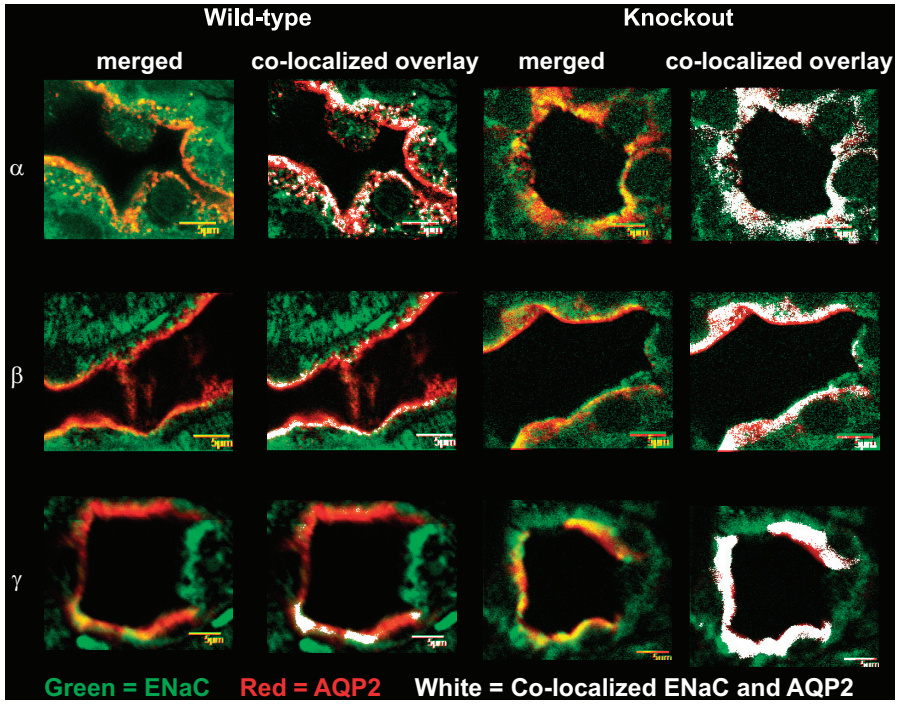

Fig. 7. ENaC subunits are in closer association with AQP2 in principal cells of KO animals than in WT animals. Kidney slices were stained with rabbit anti-ENaC subunit antibodies and goat anti-AQP2 antibody. Following treatment with appropriate fluorescent secondary antibodies, ENaC subunits (green) and AQP2 (red) were examined by confocal microscopy using an Olympus FV-1000 confocal microscope. The images in the 2 *left* columns are images from WT animals. The *left* image of the pair is a composite merged image of the red and green channels. From *top* to *bottom* are images for each of the 3 ENaC subunits. The yellow pixels in the composite image show the close association of an ENaC subunit with AQP2. The second column on the *left* is an image of the same slice as the merged image that was analyzed for colocalization of red and green pixels using a quantitative algorithm (colocalization threshold plugin in the ImageJ program; see METHODS). Pixels that have an intensity for both green and red above the green and red thresholds represent colocalization and are recolored in white. The other areas of the image represent a traditional merge of the green and red channels. Yellow areas may represent additional colocalization, but the intensities in the red and green channels are lower than the white highlighted pixels. Two *right* columns are the merged image and colocalized image for each of the 3 ENaC subunits for KO mice, respectively. There are significantly more white pixels in slices from KO animals than in WT animals ($P < 0.001$ by z-test; see Table1). Scale bars = 5 μm in all panels.

This presumably explains the increased channel density of ENaC in the apical membrane of principal cells.

Blood pressure is increased in PKCα knockout mice. If the increase in ENaC activity in knockout mice is accompanied by increased distal nephron sodium transport, then one might expect that the blood pressure of knockout mice would be elevated above that in wild-type mice. In particular, challenging the mice with a high-sodium diet should increase blood pressure. Figure 10 shows that when blood pressure was measured by tail cuff (as described in METHODS), wild-type mice challenged with a high-salt diet (8% NaCl) for 2 wk had little if any change in blood pressure while blood pressure in knockout mice increased dramatically.

ENaC activity in PKCα knockout mice on a high-salt diet. ENaC activity was recorded from cell-attached patches on principal cells (as in Figs. 1 and 3) from wild-type mice or from PKCα knockout mice fed a high-salt diet (Fig. 11*A*). The *top* two traces are long representative records from tubular cells from wild-type or knockout tubules. ENaC activity in the knockout cells is substantially increased above that in the wild-type. Figure 11, *B–D*, summarizes the results from patches on a large number of tubules from both wild-type and knockout mice. Wild-type data are from 33 individual patches; knockout data are from 42 individual patches. The patches were from 11 cortical collecting ducts isolated from WT and 15 cortical collecting ducts from PKCα KO. The cortical collect-

Table 1. *Colocalization of ENaC subunits with AQP2 in wild-type and knockout mice*

	Images	AQP2 with ENaC	ENaC with AQP2	Number of Colocalized Pixels	% Colocalized pixels
		Manders coefficients			
α	Knockout AQP2 vs. α−ENaC	0.915	0.849	6,673	15.6%
	WT AQP2 vs. α−ENaC	0.951	0.568	3,196	7.66%
β	Knockout AQP2 vs. β−ENaC	0.923	0.801	4,162	9.88%
	WT AQP2 vs. β−ENaC	0.896	0.668	1,099	2.61%
γ	Knockout AQP2 vs. γ−ENaC	0.955	0.802	7,197	13.6%
	WT AQP2 vs. γ−ENaC	0.910	0.773	1,345	2.58%

ENaC, epithelial Na channel; AQP2, aquaporin-2; WT, wild-type.

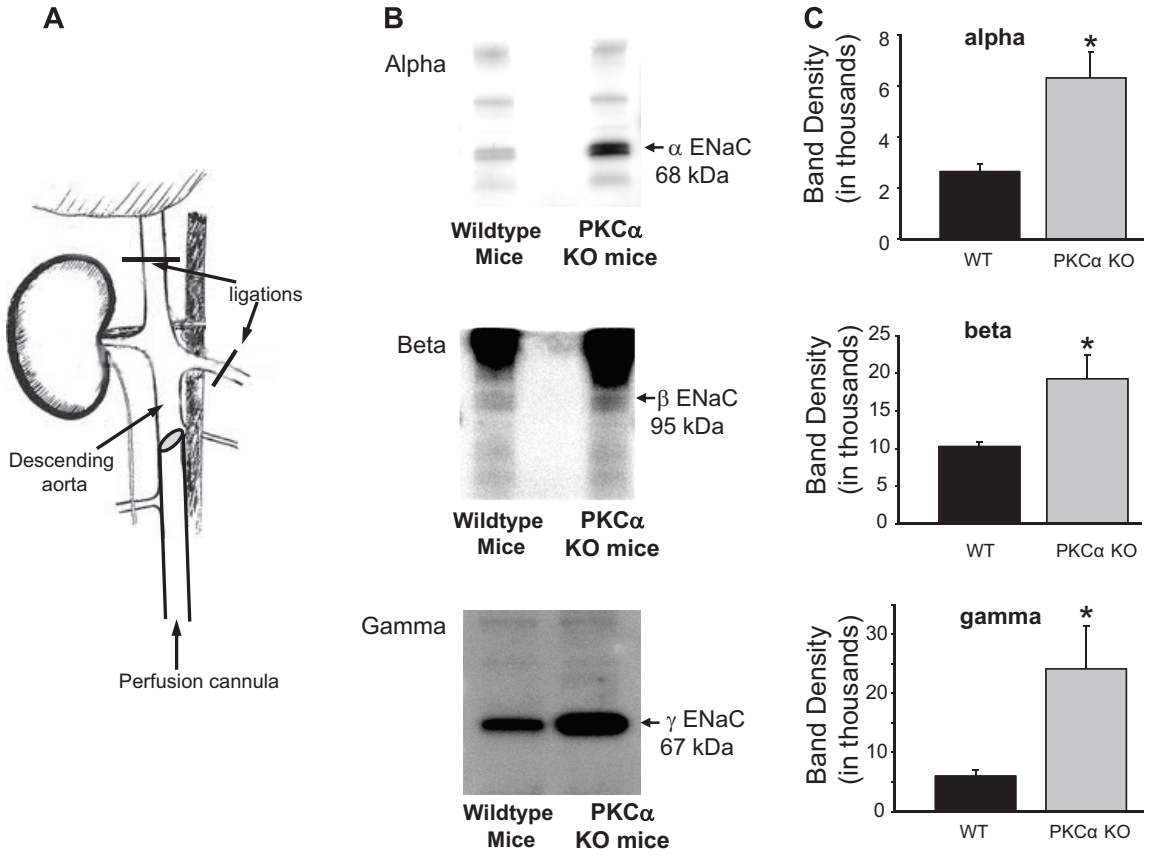

Fig. 8. In situ biotinylation of mouse kidney. *A*: schematic of the method. Mice were anesthetized by injection of 80–90 mg/kg pentobarbital sodium (ip). The abdominal cavity was opened to the diaphragm, and a butterfly needle was inserted into the abdominal aorta at the bifurcation of the iliac arteries. The aorta was tied above the level of the renal arteries, and the left renal vein was cut to allow exit of the perfusate. Both kidneys were perfused with PBS for 5 min, after which the left renal artery and vein were tied and the left kidney was removed to serve as a nonbiotinylated control. The right renal vein was then cut, and the right kidney perfused with PBS containing 0.5 mg/ml sulfosuccinimidyl-2-[biotinamido]ethyl-1,3-dithiopropionate (Pierce) for 5 min, after which a biotin-quenching solution was perfused for 25 min to remove excess biotin. *B*: biotinylated ENaC subunits. Whole kidneys were homogenized, and protein was extracted. A membrane fraction was equally loaded on streptavidin beads and incubated overnight. After washing, protein was eluted with sample buffer and resolved on gels and detected with ENaC-specific antibodies. The amount of each of the subunits was greater in the PKCα KO mice than WT. *C*: quantification of the amounts of ENaC subunits. Mean densitometric analysis is shown of 3 typical experiments for each subunit. We used ImageJ to quantify the blots. The program calculated the cumulative sum of the pixel values above the background for specific bands. Asterisks indicate significant differences in KO density compared with wild-type (by *t*-test: α-ENaC: $P = 0.026$; β-ENaC: $P = 0.046$; by rank sum test: γ-ENaC: $P = 0.029$).

ing ducts were obtained from four wild-type mice and four PKCα knockout mice. ENaC activity, measured as NP_o, the product of the number of channels (N) times P_o, is approximately doubled from 0.170 ± 0.0386 in wild-type to 0.327 ± 0.0566 in knockout ($P = 0.033$) (Fig. 11*B*). When we examined the individual components of activity, we found that P_o increased ~50% from 0.101 ± 0.0180 to 0.152 ± 0.0186 ($P = 0.028$) (Fig. 11*C*). The number of channels per patch also increased by a small but significant amount (Fig. 11*D*) from 1.35 ± 0.097 to 1.67 ± 0.095 ($P = 0.023$). Interestingly, in the knockout but not the wild-type animals, we observed several patches with more channels than we could easily measure (>12). This implies that NP_o, N, and P_o might have all been underestimated in the knockout animals.

DISCUSSION

The effect of PKC on distal nephron ENaC has been previously described in the literature (7, 15, 23, 23, 40, 49). With a few exceptions, previous reports using cultured cells have generally shown that PKC activity inhibits ENaC. Interestingly, despite the role of PKC as a protein kinase, ENaC does not appear to be directly phosphorylated by PKC (48, 49). Therefore, PKC must act indirectly to phosphorylate one or more ENaC-regulatory proteins. The purpose of this work was to investigate which proteins might be modulated by PKC to alter ENaC activity.

We were particularly interested in the PKCα knockout animals because, while there are several different renal PKC isoforms, principal cells appear to contain mostly the α-isoform. Originally, it was reported that there were no PKC isoforms in principal cells (29). Subsequently, it was shown that principal cells did contain PKCα but no other conventional isoforms (β or γ) or novel isoforms (δ, ε, θ, or η) (22). However, there is evidence for at least one atypical isoform (ζ) (19); however, the atypical isoforms usually are associated with regulation of nuclear gene expression so that only the α-isoform appears relevant to membrane signaling. Therefore, we concentrated on PKCα signaling mechanisms. In our work, we also show (Fig. 2) that PKCα is ubiquitously expressed in the kidney of wild-type mice (including AQP2-positive prin-

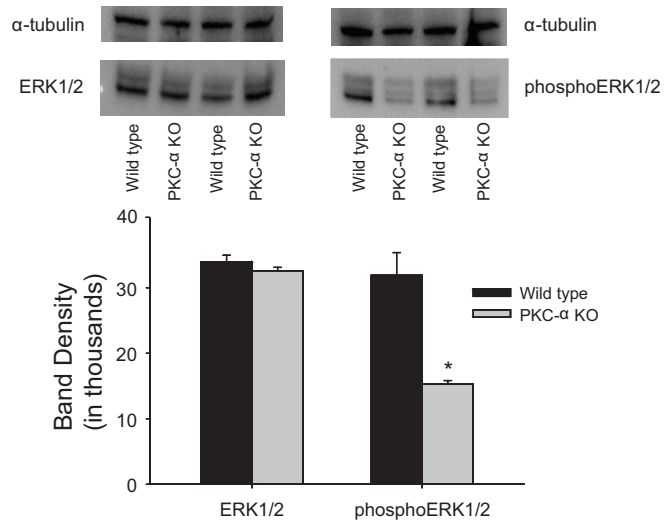

Fig. 9. Active ERK is reduced in PKCα KO mice. We measured total ERK1/2 and phosphoERK in kidney lysates (each lane represents a separate animal). We used ImageJ to quantify the blots using a area that included both ERK1 and ERK2 bands. The program calculated the cumulative sum of the pixel values above the background for specific bands. The mean values of the densitometry results from 3 separate experiments show that total ERK is the same (*t*-test, $P = 0.59$), but phosphoERK is significantly reduced in KO compared with WT mice (t test, $P < 0.001$).

cipal cells) but is not detectable in knockout mice, confirming the previous work of Madsen and coworkers (22).

ENaC P_o is increased in PKCa knockout mice. Previous work examining the effects of PKC activation or inhibition on single ENaC all suggested that there was an effect on channel P_o: PKC activation decreased P_o; PKC inhibition increased P_o (5, 7, 23, 24, 40, 48, 49). Therefore, it was not surprising to us that in principal cells in which PKC was knocked out P_o should be increased. It was interesting, however, that knocking out only one isoform, PKCα, was sufficient to produce an increase in P_o as large as any seen in previous work using inhibitors that inhibited all typical and most novel isoforms of PKC. However, in retrospect, given that PKCα appears to be the only isoform present in AQP2-positive principal cells, the significant effect of knockout on P_o might be expected. On the other hand, in other sodium-transporting epithelia that express multiple PKC isoforms (such as in the lung), the effect of knocking out only PKCα might have much more complicated effects. The mechanism by which P_o is increased likely involves phosphatidylinositol 4,5-bisphosphate (PIP_2) interaction with the channel. That ENaC gating depends upon PIP_2 has been well known for a long time (20, 25–27, 30, 50, 52). Recently, however, Alli et al. (1) have shown that the local concentration of PIP_2 in the membrane is controlled by association with the apical membrane of a specialized protein, myristoylated alanine-rich C-kinase substrate (MARCKS; or the very similar MARCKS-related protein). The ability of MARCKS to control the local concentration of PIP_2 in the membrane near ENaC depends upon the state of MARCKS phosphorylation: *1*) when dephosphorylated MARCKS associates with the membrane and membrane PIP_2 concentrations are elevated, which leads to increased ENaC P_o; and *2*) when phosphorylated MARCKS leaves the membrane and enters the cytosol, which reduces PIP_2 concentrations near ENaC, after which ENaC activity decreases. The primary kinase that phosphorylates MARCKS is PKCα. Thus, in the absence of PKCα, MARCKS remains associated with the membrane and increases PIP_2 concentrations near ENaC and ENaC P_o increases (as we observed).

ENaC membrane density is increased in PKCa knockout mice. Besides an increase in P_o, we also observed an increase in the membrane density of ENaC. While it might be possible that increased PIP_2 in the apical membrane alone could stabilize ENaC and allow an accumulation in the membrane, other mechanisms appear to contribute. Activation of PKC with phorbol esters is known to reduce ENaC subunit protein in the membrane (7, 40). It is also known that phosphorylation of ENaC by the active, phosphorylated form of ERK1/2 does promote interaction of ENaC with the ubiquitin ligase (7) Nedd4-2. Nedd4-2 ubiquitination promotes ENaC removal from the membrane and internalization, reducing the overall levels of ENaC in the membrane (21, 32). PKC can phosphorylate and activate ERK1/2 (7, 10). We showed that in the absence of PKCα the active phosphorylated form of ERK1/2 was significantly reduced, thereby leading to reduced ENaC internalization and to the increase in membrane ENaC we observed.

Blood pressure is elevated in PKCa knockout mice. One might expect that if there are substantial increases in distal nephron sodium reabsorption, there would be a concomitant increase in blood volume and blood pressure. One previous study did not observe any significant difference in blood pressure between wild-type and PKCα knockout mice (43). However, those experiments were done on mice fed a normal-salt diet, which might not reveal a sodium balance problem. Even mice with a mutation which produces constitutively active ENaC do not have noticeably elevated blood pressure in the absence of a high-salt challenge (31). Therefore, we fed our mice an 8% sodium chloride diet and did observe a significant increase in blood pressure in the knockout animals. We con-

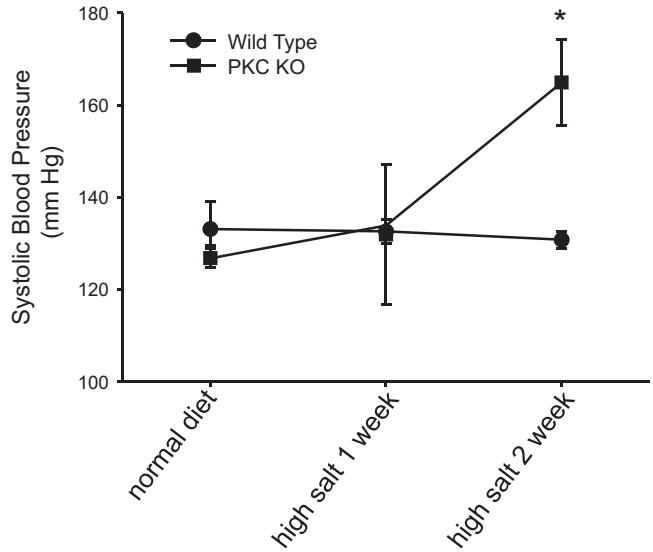

Fig. 10. Blood pressure is increased in PKCα knockout mice. When blood pressure was measured by tail cuff (as described in METHODS), WT mice challenged with a high-salt diet (8% NaCl) had little if any change in systolic blood pressure, while blood pressure in KO mice increased significantly (marked with asterisk; $n = 4$/group). $P < 0.001$ for *week 2* on a high-salt for KO vs. WT by 2-way ANOVA.

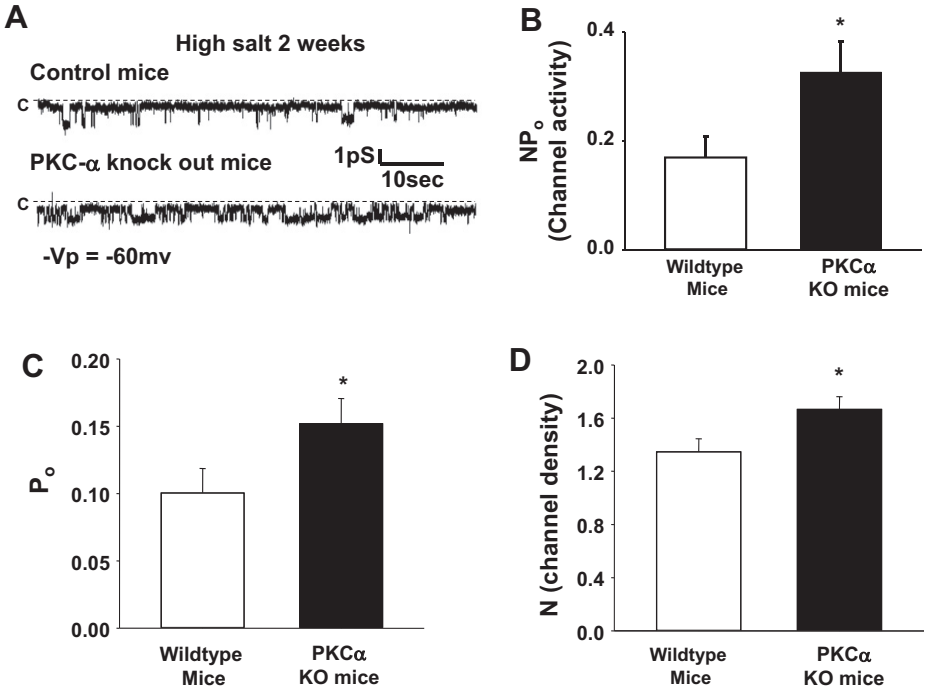

Fig. 11. ENaC activity from tubules in high-salt diet mice. ENaC activity was recorded from cell-attached patches on principal cells (as in Figs. 1 and 3) from WT mice or PKCα KO mice. *A*: *top* trace is a representative record from WT, and *bottom* trace from a KO cell. The activity of the KO cell is substantially increased above that of the WT. All recordings were made at −60 mV (difference in potential between the inside of the cell and the patch pipette. If there is a significant basal membrane potential, it will add to the pipette potential). *B–D*: summary of all single-channel data The graph in *B* shows that ENaC NP_o [measured as the number of channels (*N*) times the P_o] increases ~50% in the PKCα KO mice compared with WT ($P = 0.033$). When the components of activity are examined individually, both P_o (*C*) and *N* (*D*) increase significantly ($P < 0.03$). WT data are from 33 individual patches; KO data are from 42 individual patches. The patches were from 11 cortical collecting ducts isolated from WT and 15 cortical collecting ducts from PKCα KO. The cortical collecting ducts were obtained from 4 WT mice and 4 PKCα KO mice.

firmed using single-channel measurements that ENaC activity in knockout animals was increased and could, therefore, account for the high blood pressure.

Figure 12 shows a schematic diagram of PKC signaling in wild-type and knockout mice. The situation in wild-type mice is shown in Fig. 12*A*. PKCα is active and phosphorylates MARCKS protein. When phosphorylated, MARCKS leaves the membrane and does not sequester and present PIP_2 to ENaC, causing ENaC P_o to decrease. Active PKC also phosphorylates ERK, which in turn phosphorylates ENaC. ERK phosphorylation of ENaC promotes Nedd4-2 interaction with and ubiquitination of ENaC, with subsequent internalization. This reduces the apical density of ENaC. The situation in PKCα knockout mice is shown in Fig. 12*B*. PKC is absent, and MARCKS protein is not phosphorylated. Therefore, MARCKS remains associated with the membrane and presents PIP_2 to ENaC to increase ENaC P_o. ERK is also not phosphorylated so that ENaC internalization is reduced and apical membrane ENaC is increased.

A recent genome-wide association study (44) found that polymorphic changes in only a very limited number of genes were associated with increases in blood pressure. The strongest linkage involved polymorphisms in the gene for PKCα. The study provides no information about the specific effects that the polymorphisms have on PKC activity. We speculate based on our results that the polymorphisms lead to decreases in PKC activity. We will be interested in expressing specific PKC mutations in heterologous expression systems that also express ENaC to determine the effect of the polymorphisms on ENaC activity.

Our work has shown an important role for PKCα in the regulation of ENaC with a potential for significant hypertension in animals or patients with reduced PKC activity. One therapeutic agent in common use, rapamycin, is a PKC inhib-

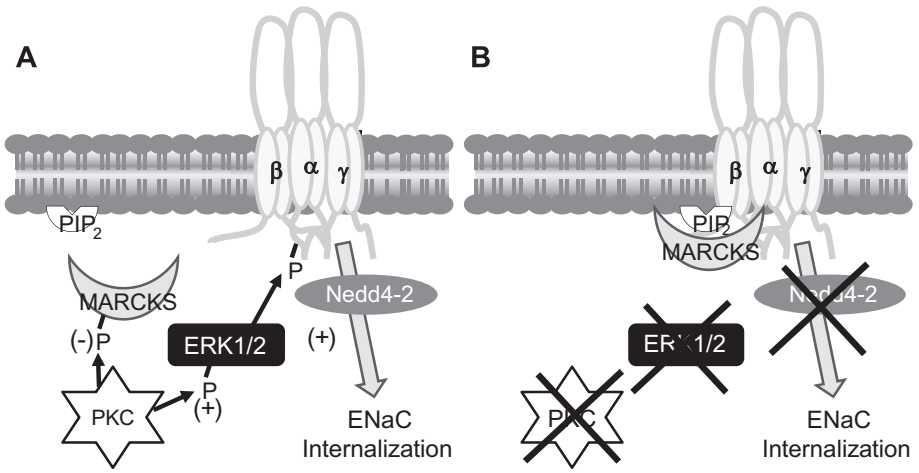

Fig. 12. Schematic diagram of PKC signaling in WT and KO mice. *A*: situation in WT mice. PKCα is active and phosphorylates myristoylated alanine-rich C-kinase substrate (MARCKS) protein. When phosphorylated, MARCKS leaves the membrane and does not sequester and present phosphatidylinositol 4,5-bisphosphate (PIP_2) to ENaC, causing a decrease in ENaC P_o. Active PKC also phosphorylates ERK, which in turn phosphorylates ENaC. ERK phosphorylation of ENaC promotes Nedd4-2 interaction with and ubiquitination of ENaC, with subsequent internalization. This reduces the apical density of ENaC. *B*: situation in PKCα KO mice. PKC is absent, and MARCKS protein is not phosphorylated. Therefore, MARCKS remains associated with the membrane and presents PIP_2 to ENaC to increase ENaC P_o. ERK is also not phosphorylated so that ENaC internalization is reduced and apical membrane ENaC is increased.

itor (49) and does commonly induce hypertension (42). Given the examination of PKC inhibitors for a variety of clinical disorders (36, 38, 51), it seems appropriate to understand the mechanisms by which the inhibitors can produce excessive renal sodium transport and hypertension.

GRANTS

This work was supported by National Institutes of Health Grants R37 DK037963 to D. C. Eaton, R01 DK89828 to J. M. Sands, R01-DK067110 to H.-P. Ma, and T32 DK07656 and AHA 13POST16820072 to T. L. Thai.

DISCLOSURES

No conflicts of interest, financial or otherwise, are declared by the authors.

AUTHOR CONTRIBUTIONS

Author contributions: H.-F.B., H.-P.M., H.C., J.D.K., J.M.S., and D.C.E. provided conception and design of research; H.-F.B., T.L.T., and Q.Y. performed experiments; H.-F.B., T.L.T., Q.Y., A.F.E., and D.C.E. analyzed data; H.-F.B., T.L.T., H.-P.M., J.D.K., J.M.S., and D.C.E. interpreted results of experiments; H.-F.B., T.L.T., A.F.E., and D.C.E. prepared figures; H.-F.B., T.L.T., H.-P.M., A.F.E., H.C., J.D.K., J.M.S., and D.C.E. edited and revised manuscript; H.-F.B., T.L.T., Q.Y., H.-P.M., A.F.E., H.C., J.D.K., J.M.S., and D.C.E. approved final version of manuscript; D.C.E. drafted manuscript.

REFERENCES

1. **Alli AA, Bao HF, Alli AA, Aldrugh Y, Song JZ, Ma HP, Yu L, Al-Khalili O, Eaton DC.** Phosphatidylinositol phosphate-dependent regulation of Xenopus ENaC by MARCKS protein. *Am J Physiol Renal Physiol* 303: F800–F811, 2012.
2. **Alli AA, Gower WR Jr.** The C type natriuretic peptide receptor tethers AHNAK1 at the plasma membrane to potentiate arachidonic acid-induced calcium mobilization. *Am J Physiol Cell Physiol* 297: C1157–C1167, 2009.
3. **Alli AA, Gower WR Jr.** Molecular approaches to examine the phosphorylation state of the C type natriuretic peptide receptor. *J Cell Biochem* 110: 985–994, 2010.
4. **Alli AA, Song JZ, Al-Khalili O, Bao HF, Ma HP, Alli AA, Eaton DC.** Cathepsin B is secreted apically from Xenopus 2F3 cells and cleaves the epithelial sodium channel (ENaC) to increase its activity. *J Biol Chem* 287: 30073–30083, 2012.
5. **Awayda MS, Ismailov II, Berdiev BK, Fuller CM, Benos DJ.** Protein kinase regulation of a cloned epithelial Na+ channel. *J Gen Physiol* 108: 49–65, 1996.
6. **Bao HF, Zhang ZR, Liang YY, Ma JJ, Eaton DC, Ma HP.** Ceramide mediates inhibition of the renal epithelial sodium channel by tumor necrosis factor-α through protein kinase C. *Am J Physiol Renal Physiol* 293: F1178–F1186, 2007.
7. **Booth RE, Stockand JD.** Targeted degradation of ENaC in response to PKC activation of the ERK1/2 cascade. *Am J Physiol Renal Physiol* 284: F938–F947, 2003.
8. **Bou Matar RN, Malik B, Wang XH, Martin CF, Eaton DC, Sands JM, Klein JD.** Protein abundance of urea transporters and aquaporin 2 change differently in nephrotic pair-fed vs. non-pair-fed rats. *Am J Physiol Renal Physiol* 302: F1545–F1553, 2012.
9. **Chang SS, Grunder S, Hanukoglu A, Rosler A, Mathew PM, Hanukoglu I, Schild L, Lu Y, Shimkets RA, Nelson-Williams C, Rossier BC, Lifton RP.** Mutations in subunits of the epithelial sodium channel cause salt wasting with hyperkalaemic acidosis, pseudohypoaldosteronism type 1. *Nat Genet* 12: 248–253, 1996.
10. **Corbit KC, Trakul N, Eves EM, Diaz B, Marshall M, Rosner MR.** Activation of Raf-1 signaling by protein kinase C through a mechanism involving Raf kinase inhibitory protein. *J Biol Chem* 278: 13061–13068, 2003.
11. **Dunn KW, Kamocka MM, McDonald JH.** A practical guide to evaluating colocalization in biological microscopy. *Am J Physiol Cell Physiol* 300: C723–C742, 2011.
12. **Frindt G, Ergonul Z, Palmer LG.** Surface expression of epithelial Na channel protein in rat kidney. *J Gen Physiol* 131: 617–627, 2008.
13. **Frindt G, Palmer LG.** Na channels in the rat connecting tubule. *Am J Physiol Renal Physiol* 286: F669–F674, 2004.
14. **Frindt G, Palmer LG.** Surface expression of sodium channels and transporters in rat kidney: effects of dietary sodium. *Am J Physiol Renal Physiol* 297: F1249–F1255, 2009.
15. **Frindt G, Palmer LG, Windhager EE.** Feedback regulation of Na channels in rat CCT. IV. Mediation by activation of protein kinase C. *Am J Physiol Renal Fluid Electrolyte Physiol* 270: F371–F376, 1996.
16. **Garty H, Palmer LG.** Epithelial sodium channels: function, structure, and regulation. *Physiol Rev* 77: 359–396, 1997.
17. **Hambleton M, Hahn H, Pleger ST, Kuhn MC, Klevitsky R, Carr AN, Kimball TF, Hewett TE, Dorn GW, Koch WJ, Molkentin JD.** Pharmacological- and gene therapy-based inhibition of protein kinase Calpha/beta enhances cardiac contractility and attenuates heart failure. *Circulation* 114: 574–582, 2006.
18. **Hansson JH, Nelson-Williams C, Suzuki H, Schild L, Shimkets RA, Lu Y, Canessa CM, Iwasaki T, Rossier BC, Lifton RP.** Hypertension caused by a truncated epithelial sodium channel gamma subunit: genetic heterogeneity of Liddle syndrome. *Nat Genet* 11: 76–82, 1995.
19. **Hao CM, Breyer RM, Davis LS, Breyer MD.** Intrarenal distribution of rabbit PKC zeta. *Kidney Int* 51: 1831–1837, 1997.
20. **Helms MN, Liu L, Liang YY, Al-Khalili O, Vandewalle A, Saxena S, Eaton DC, Ma HP.** Phosphatidylinositol 3,4,5-trisphosphate mediates aldosterone stimulation of epithelial sodium channel (ENaC) and interacts with gamma-ENaC. *J Biol Chem* 280: 40885–40891, 2005.
21. **Kabra R, Knight KK, Zhou R, Snyder PM.** Nedd4–2 induces endocytosis and degradation of proteolytically cleaved epithelial Na^+ channels. *J Biol Chem* 283: 6033–6039, 2008.
22. **Kim WY, Jung JH, Park EY, Yang CW, Kim H, Nielsen S, Madsen KM, Kim J.** Expression of protein kinase C isoenzymes alpha, betaI, and delta in subtypes of intercalated cells of mouse kidney. *Am J Physiol Renal Physiol* 291: F1052–F1060, 2006.
23. **Ling BN, Eaton DC.** Effects of luminal Na^+ on single Na^+ channels in A6 cells, a regulatory role for protein kinase C. *Am J Physiol Renal Fluid Electrolyte Physiol* 256: F1094–F1103, 1989.
24. **Ling BN, Kokko KE, Eaton DC.** Inhibition of apical Na+ channels in rabbit cortical collecting tubules by basolateral prostaglandin E2 is modulated by protein kinase C. *J Clin Invest* 90: 1328–1334, 1992.
25. **Ma HP, Chou CF, Wei SP, Eaton DC.** Regulation of the epithelial sodium channel by phosphatidylinositides: experiments, implications, and speculations. *Pflügers Arch* 455: 169–180, 2007.
26. **Ma HP, Eaton DC.** Acute regulation of epithelial sodium channel by anionic phospholipids. *J Am Soc Nephrol* 16: 3182–3187, 2005.
27. **Ma HP, Saxena S, Warnock DG.** Anionic phospholipids regulate native and expressed ENaC. *J Biol Chem* 277: 7641–7644, 2002.
28. **Manders EMM, Vereek FJ, Aten JA.** Measurement of co-localization of objects in dual-colour confocal images. *J Microsc* 169: 375–382, 1993.
29. **Pfaff IL, Wagner HJ, Vallon V.** Immunolocalization of protein kinase C isoenzymes alpha, beta1 and betaII in rat kidney. *J Am Soc Nephrol* 10: 1861–1873, 1999.
30. **Pochynyuk O, Tong Q, Staruschenko A, Ma HP, Stockand JD.** Regulation of the epithelial Na^+ channel (ENaC) by phosphatidylinositides. *Am J Physiol Renal Physiol* 290: F949–F957, 2006.
31. **Pradervand S, Wang Q, Burnier M, Beermann F, Horisberger JD, Hummler E, Rossier BC.** A mouse model for Liddle's syndrome. *J Am Soc Nephrol* 10: 2527–2533, 1999.
32. **Raikwar NS, Thomas CP.** Nedd4–2 isoforms ubiquitinate individual epithelial sodium channel subunits and reduce surface expression and function of the epithelial sodium channel. *Am J Physiol Renal Physiol* 294: F1157–F1165, 2008.
33. **Schild L.** The ENaC channel as the primary determinant of two human diseases: Liddle syndrome and pseudohypoaldosteronism. *Nephrologie* 17: 395–400, 1996.
34. **Schild L.** The epithelial sodium channel: from molecule to disease. *Rev Physiol Biochem Pharmacol* 151: 93–107, 2004.
35. **Schneider CA, Rasband WS, Eliceiri KW.** NIH Image to ImageJ: 25 years of image analysis. *Nat Methods* 9: 671–675, 2012.
36. **Shen GX.** Selective protein kinase C inhibitors and their applications. *Curr Drug Targets Cardiovasc Haematol Disord* 3: 301–307, 2003.
37. **Shimkets RA, Warnock DG, Bositis CM, Nelson-Williams C, Hansson JH, Schambelan M, Gill JR Jr, Ulick S, Milora RV, Findling JW, Canessa CM, Rossier BC, Lifton RP.** Liddle's syndrome: heritable human hypertension caused by mutations in the B subunit of the epithelial sodium channel. *Cell* 79: 407–414, 1994.
38. **Skvara H, Dawid M, Kleyn E, Wolff B, Meingassner JG, Knight H, Dumortier T, Kopp T, Fallahi N, Stary G, Burkhart C, Grenet O,**

Wagner J, Hijazi Y, Morris RE, McGeown C, Rordorf C, Griffiths CE, Stingl G, Jung T. The PKC inhibitor AEB071 may be a therapeutic option for psoriasis. *J Clin Invest* 118: 3151–3159, 2008.

39. **Snyder PM.** Minireview: regulation of epithelial Na^+ channel trafficking. *Endocrinology* 146: 5079–5085, 2005.
40. **Stockand JD, Bao HF, Schenck J, Malik B, Middleton P, Schlanger LE, Eaton DC.** Differential effects of protein kinase C on the levels of epithelial Na^+ channel subunit proteins. *J Biol Chem* 275: 25760–25765, 2000.
41. **Strautnieks SS, Thompson RJ, Hanukoglu A, Dillon MJ, Hanukoglu I, Kuhnle U, Seckl J, Gardiner RM, Chung E.** Localisation of pseudohypoaldosteronism genes to chromosome 16p12.2–1311 and 12p131-pter by homozygosity mapping. *Hum Mol Genet* 5: 293–299, 1996.
42. **Sundaram V, Abraham G, Sundaram V, Mathew M, Bhaskar S, Ponnusamy J, Prabu S.** Rapamycin-induced hypokalaemic nephropathy in a middle-aged hypertensive male. *Nephrol Dial Transplant* 22: 1798, 2007.
43. **Thai TL, Blount MA, Klein JD, Sands JM.** Lack of protein kinase C-α leads to impaired urine concentrating ability and decreased aquaporin-2 in angiotensin II-induced hypertension. *Am J Physiol Renal Physiol* 303: F37–F44, 2012.
44. **Turner ST, Boerwinkle E, O'Connell JR, Bailey KR, Gong Y, Chapman AB, McDonough CW, Beitelshees AL, Schwartz GL, Gums JG, Padmanabhan S, Hiltunen TP, Citterio L, Donner KM, Hedner T, Lanzani C, Melander O, Saarela J, Ripatti S, Wahlstrand B, Manunta P, Kontula K, Dominiczak AF, Cooper-DeHoff RM, Johnson JA.** Genomic association analysis of common variants influencing antihypertensive response to hydrochlorothiazide. *Hypertension* 62: 391–397, 2013.
45. **Yu L, Bao HF, Self JL, Eaton DC, Helms MN.** Aldosterone-induced increases in superoxide production counters nitric oxide inhibition of epithelial Na channel activity in A6 distal nephron cells. *Am J Physiol Renal Physiol* 293: F1666–F1677, 2007.
46. **Yu L, Cai H, Yue Q, Alli AA, Wang D, Al-Khalili O, Bao HF, Eaton DC.** WNK4 inhibition of ENaC is independent of Nedd4-2-mediated ENaC ubiquitination. *Am J Physiol Renal Physiol* 305: F31–F41, 2013.
47. **Yu L, Eaton DC, Helms MN.** Effect of divalent heavy metals on epithelial Na^+ channels in A6 cells. *Am J Physiol Renal Physiol* 293: F236–F244, 2007.
48. **Yue G, Eaton DC.** Protein kinase C does not affect epithelial Na^+ channel activity in inside-out patches from A6 cells (Abstract). *FASEB J* 12: A179. 1998.
49. **Yue G, Edinger RS, Bao HF, Johnson JP, Eaton DC.** The effect of rapamycin on single ENaC channel activity and phosphorylation in A6 cells. *Am J Physiol Cell Physiol* 279: C81–C88, 2000.
50. **Yue G, Malik B, Yue G, Eaton DC.** Phosphatidylinositol 4,5-bisphosphate (PIP2) stimulates epithelial sodium channel activity in A6 cells. *J Biol Chem* 277: 11965–11969, 2002.
51. **Zarate CA, Manji HK.** Protein kinase C inhibitors: rationale for use and potential in the treatment of bipolar disorder. *CNS Drugs* 23: 569–582, 2009.
52. **Zhang ZR, Chou CF, Wang J, Liang YY, Ma HP.** Anionic phospholipids differentially regulate the epithelial sodium channel (ENaC) by interacting with alpha, beta, and gamma ENaC subunits. *Pflügers Arch* 459: 377–387, 2010.
53. **Zhou R, Patel SV, Snyder PM.** Nedd4–2 catalyzes ubiquitination and degradation of cell surface ENaC. *J Biol Chem* 282: 20207–20212, 2007.